

Electronic Supplementary Information

Experimental section

Materials: GO, ammonium chloride (NH_4Cl), hydrazine hydrate ($\text{N}_2\text{H}_4\cdot\text{H}_2\text{O}$), sodium hypochlorite (NaClO), sodium hydroxide (NaOH), sodium salicylate ($\text{C}_7\text{H}_5\text{O}_3\text{Na}$), Lithium Perchlorate (LiClO_4), hydrochloric acid (HCl), ethanol ($\text{CH}_3\text{CH}_2\text{OH}$), and carbon paper were bought from Beijing Chemical Corporation. Potassium hexachloropalladate (IV) and red phosphorus were obtained from Macklin Chemical Reagent Co, Ltd. Para-(dimethylamino) benzaldehyde ($\text{C}_9\text{H}_{11}\text{NO}$), sodium nitroferricyanide (III) dihydrate ($\text{Na}_2\text{Fe}(\text{CN})_5\text{NO}\cdot 2\text{H}_2\text{O}$), and Nafion were purchased from Aladdin Ltd. (Shanghai, China). The water used throughout all experiments was purified through a Millipore system.

Preparation of Pd-GO: 5 mL (8 mg/L) K_2PdCl_6 (0.1 mmol) solution was inserted into 100 mL of GO solution (0.5 mg/mL) with stirring for 3 h at 0°C . Then the obtained black precipitate was separated by centrifuging, and further washing was done with Millipore water. Finally, the nanocomposite sample was freeze-dried for 24 h.

Preparation of Pd-rGO: 50 mg Pd-GO was annealed in Ar atmosphere at 900°C for 2 h with a rate of $10^\circ\text{C}/\text{min}$.

Preparation of PdP₂-rGO: PdP₂-rGO was prepared by a modified high temperature solid state synthesis. The constituent elements (Pd, P) was reacted in the molar ratio 1:2. Pd-GO was placed in a separate quartz tube and red phosphorus was placed in the outer quartz tube. The quartz tube was sealed after evacuating through a vacuum line ($\sim 10^{-4}$ bar). Subsequently, the sealed tube was kept at 900°C for three days and slowly cooled to 25°C . The product was removed by breaking the tube under ambient conditions and standing for 2 h.

Preparation of PdP₂-rGO/CP electrode: 5 mg PdP₂-rGO powders and 40 μL of Nafion solution (5 wt %) were dispersed in 960 μL mixed solution contains 700 μL ethanol and 260 μL H_2O by 30 min sonication to form a homogeneous ink. Then, 20 μL of ink was loaded on a CP with an area of $1.0 \times 1.0 \text{ cm}^2$ and dried under ambient condition.

Preparation of Pd-rGO/CP electrode: 5 mg Pd-rGO powders and 40 μL of Nafion solution (5 wt %) were dispersed in 960 μL mixed solution contains 700 μL ethanol and 260 μL H_2O by 30 min sonication to form a homogeneous ink. Then, 20 μL of ink was loaded on a CP with an area of $1.0 \times 1.0 \text{ cm}^2$ and dried under ambient condition.

Characterizations: XRD patterns were obtained from a Shimadzu XRD-6100 diffractometer with Cu K α radiation (40 kV, 30 mA) of wavelength 0.154 nm (Japan). TEM images were obtained from a Zeiss Libra 200FE transmission electron microscope operated at 200 kV. XPS measurements were performed on an ESCALABMK II X-ray photoelectron spectrometer using Mg as the exciting source. Raman spectroscopy was collected on a Renishaw in confocal Raman system. The absorbance data of spectrophotometer were measured on SHIMADZU UV-1800 ultraviolet-visible (UV-Vis) spectrophotometer. The ion chromatography data were collected on Thermofisher ICS 5000 plus.

Electrochemical measurements: Electrochemical measurements were performed with a CHI 660E electrochemical analyzer (CH Instruments, Inc., Shanghai) using a standard three-electrode system using PdP₂-rGO/CP as the working electrode, graphite rod as the counter electrode, and saturated Ag/AgCl electrode as the reference electrode. In all measurements, saturated Ag/AgCl electrode was calibrated with respect to reversible hydrogen electrode as following: in 0.5 M LiClO₄ aqueous solution, $E(\text{RHE}) = E(\text{Ag}/\text{AgCl}) + 0.059 \times \text{pH} + 0.197 \text{ V}$. All experiments were carried out at room temperature. For N₂ reduction experiments, the 0.5 M LiClO₄ electrolyte was purged with N₂ for 30 min before the measurement. Potentiostatic test was conducted in N₂-saturated 0.5 M LiClO₄ solution in a two-compartment cell, which was separated by Nafion 117 membrane.

Determination of NH₃: The produced NH₃ was detected with indophenol blue by ultraviolet spectroscopy.¹ In detail, 4 mL electrolyte was obtained from the cathodic chamber and mixed with 50 μL oxidizing solution containing NaClO ($\text{pCl} = 4 \sim 4.9$) and NaOH (0.75 M), 500 μL coloring solution containing 0.4 M C₇H₅O₃Na and 0.32 M NaOH, and 50 μL catalyst solution (1 wt% Na₂[Fe(CN)₅NO]) for 1 h. Absorbance

measurements were performed at $\lambda = 650$ nm. The concentration-absorbance curve was calibrated using standard NH_4^+ solution with a series of concentrations. The fitting curve ($y = 0.628x + 0.0342$, $R^2 = 0.998$) shows good linear relation of absorbance value with NH_4^+ concentration.

Determination of N_2H_4 : The N_2H_4 present in the electrolyte was determined by the method of Watt and Chrisp.² The mixture of $\text{C}_9\text{H}_{11}\text{NO}$ (5.99 g), HCl (30 mL), and $\text{C}_2\text{H}_5\text{OH}$ (300 mL) was used as a color reagent. In detail, 5 mL electrolyte was removed from the electrochemical reaction vessel, and added into 5 mL above prepared color reagent and stirring 10 min at room temperature. Moreover, the absorbance of the resulting solution was measured at a wavelength of 455 nm. The concentration absorbance curves were calibrated using standard N_2H_4 solution with a series of concentrations. The fitting curve ($y = 0.525x + 0.1255$, $R^2 = 0.999$) shows good linear relation of absorbance value with N_2H_4 concentration.

Calculations of NH_3 yield rate and FE: NH_3 yield rate was calculated using the following equation:

$$\text{NH}_3 \text{ yield rate} = [\text{NH}_4^+] \times V / (m_{\text{cat.}} \times t)$$

FE was calculated according to the following equation:

$$\text{FE} = 3 \times F \times [\text{NH}_4^+] \times V / (18 \times Q)$$

Where $[\text{NH}_4^+]$ is the measured NH_4^+ concentration; V is the volume of the cathodic reaction electrolyte; t is the potential applied time; $m_{\text{cat.}}$ is the loaded quality of catalyst; F is the Faraday constant; Q is the quantity of applied electricity

Calculation details: The first-principles calculations in the framework of DFT (density functional theory) are carried out using the Vienna ab initio Simulation Package (VASP).^{3,4} The ion-electron interactions were described by Projector augmented wave (PAW)⁵ method. The generalized gradient approximation (GGA) in the Perdew-Burke-Ernzerhof (PBE) form^{6,7} was employed, and energy cutoff of 400 eV was set for plane-wave basis. The mainly exposed (011) surface of PdP_2 with $I_{2/c}$ space group was modeled by a 8-layer $p(3 \times 3)$ unit cell of $4.48 \text{ \AA} \times 5.82 \text{ \AA}$, and the (111) surface of Pd was modeled by a 4-layer $p(2 \times 2)$ unit cell. During the geometry optimization, the bottom four layers of PdP_2 (011) and the bottom two layers of Pd

(111) were fixed while the atomic positions of other layers and adsorbates were relaxed until the forces were converged to less than 0.03 eV \AA^{-1} . The Brillouin zones were sampled by a Gamma-center k-point mesh with a $3 \times 3 \times 1$ k-point grid, and a vacuum space of 15 \AA was employed to avoid the interaction between two periodic units. The adsorption energies (E_{ads}) of the NRR intermediates were determined by $E_{\text{ads}} = E_{\text{tot}} - E_{\text{slab}} - E_{\text{ads}}$, where E_{tot} , E_{slab} and E_{ads} represent the total energies of the species adsorbed slab system, the clean slab, and the adsorbate, respectively. According to this definition, more negative adsorption energy indicates stronger adsorption. The calculations of Gibbs free energy change (ΔG) was computed by $\Delta G = \Delta E + \Delta E_{\text{ZPE}} - T\Delta S + neU$ for each elemental step, which is based on the computational hydrogen electrode (CHE) model proposed by Nørskov et.al,⁸ where ΔE is the calculated DFT energy; ΔE_{ZPE} and ΔS are the changes in zero point energies and entropy, respectively; T is the temperature, which is set to be 298.15 K in this work; n and U are the number of electrons transferred and the electrode potential applied, respectively. In this study, the entropies of molecules in the gas phase were obtained from the NIST database.

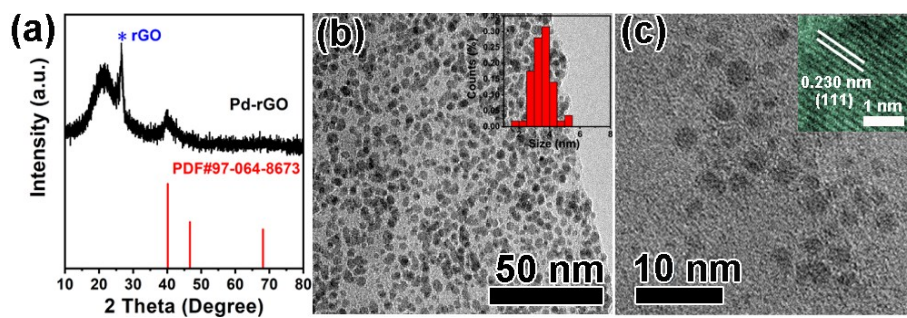


Fig. S1. (a) XRD pattern, (b) low-magnification and (c) high-magnification TEM images of the Pd-rGO (inset in c: HRTEM image taken from one single Pd particle).

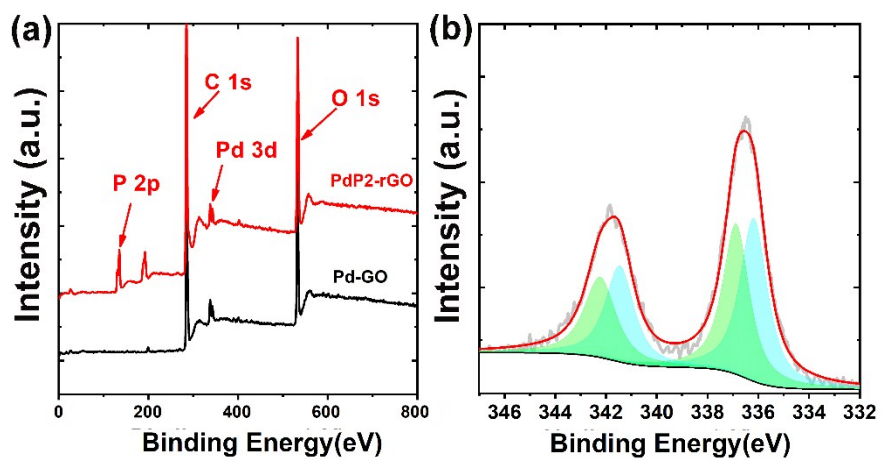


Fig. S2. (a) XPS survey spectra and (b) Pd 3d spectrum of the Pd-rGO.

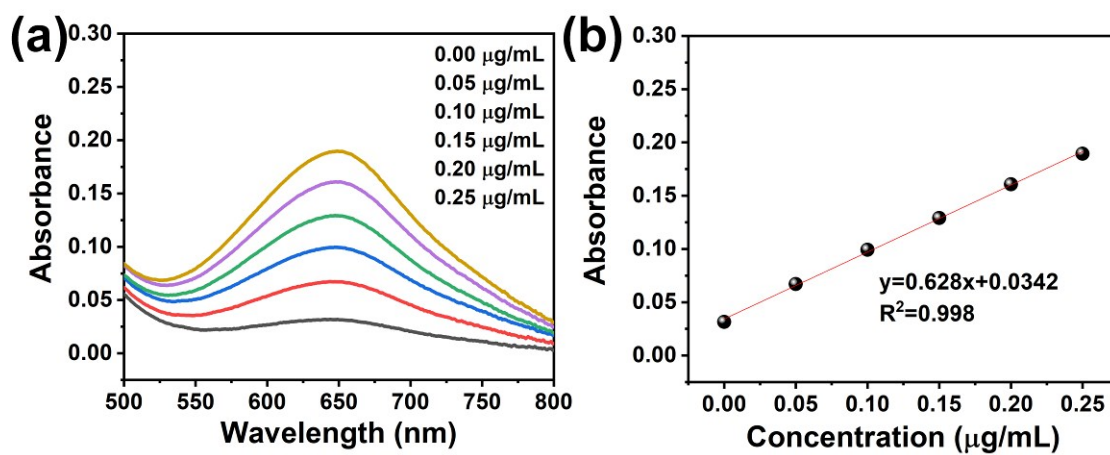


Fig. S3. (a) UV-Vis absorption spectra of indophenol assays with NH_4^+ concentrations after incubated for 1 h at room temperature. (b) Calibration curve used for calculation of NH_4^+ concentrations.

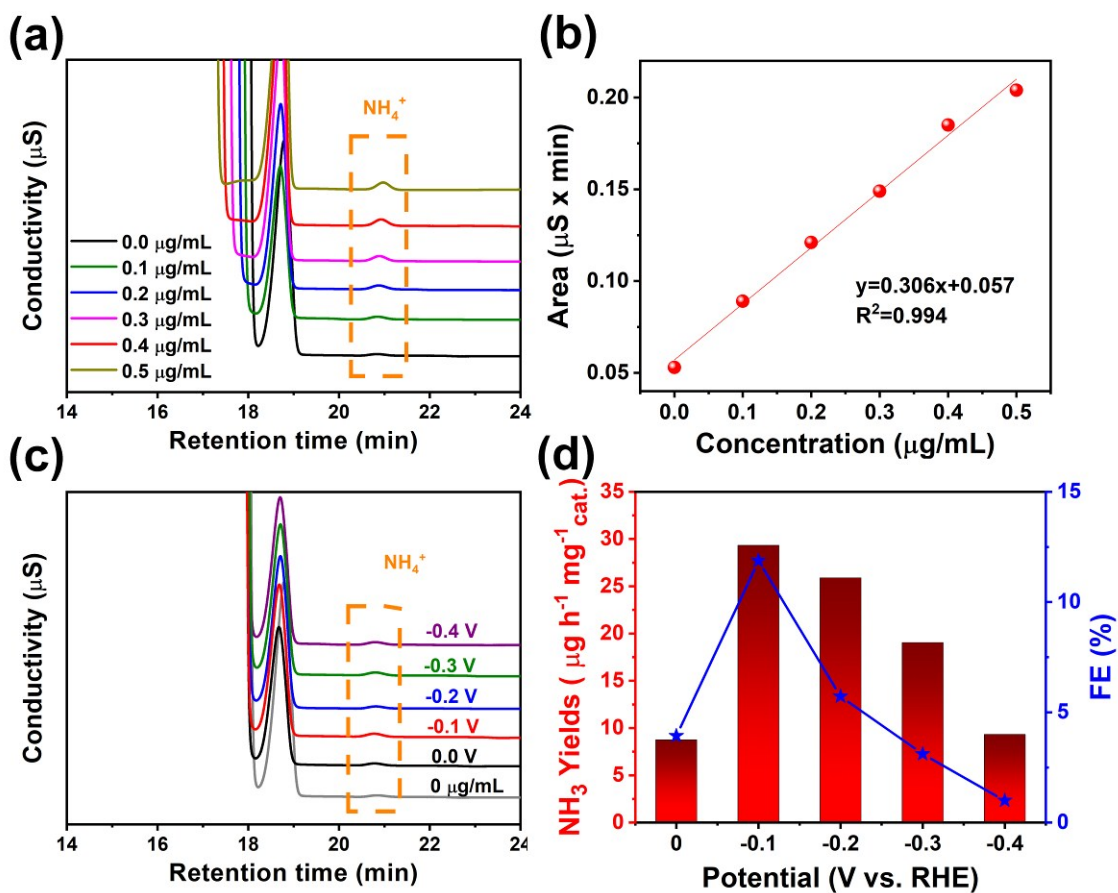


Fig. S4. (a) Ion chromatogram analysis for the NH₄⁺ ions. (b) Calibration curve used for estimation of NH₄⁺. (c) Ion chromatogram data for the electrolytes at a series of potentials after electrolysis for 2 h. (d) NH₃ yields and FEs for PdP₂-rGO/CP at corresponding potentials.

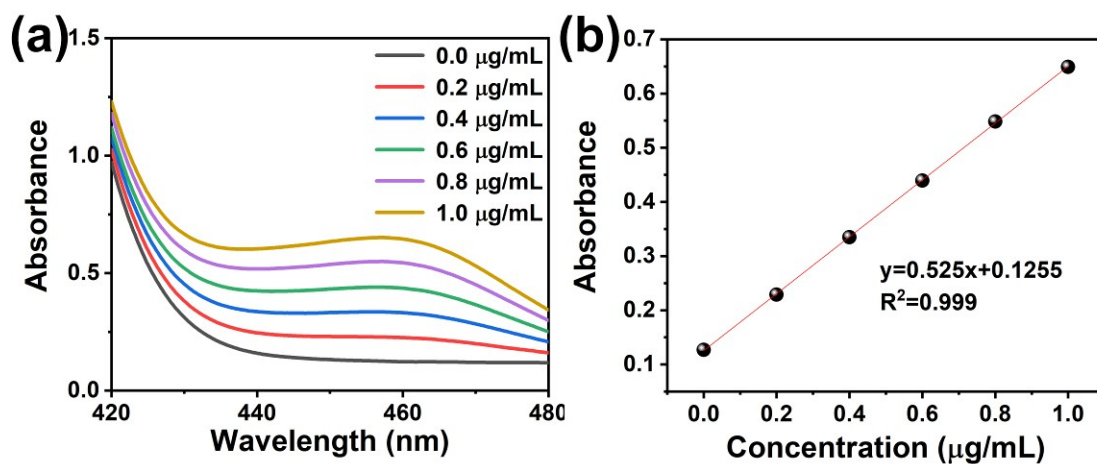


Fig. S5. (a) UV-Vis absorption spectra of various N_2H_4 concentrations after incubated for 10 min at room temperature. (b) Calibration curve used for calculation of N_2H_4 concentrations.

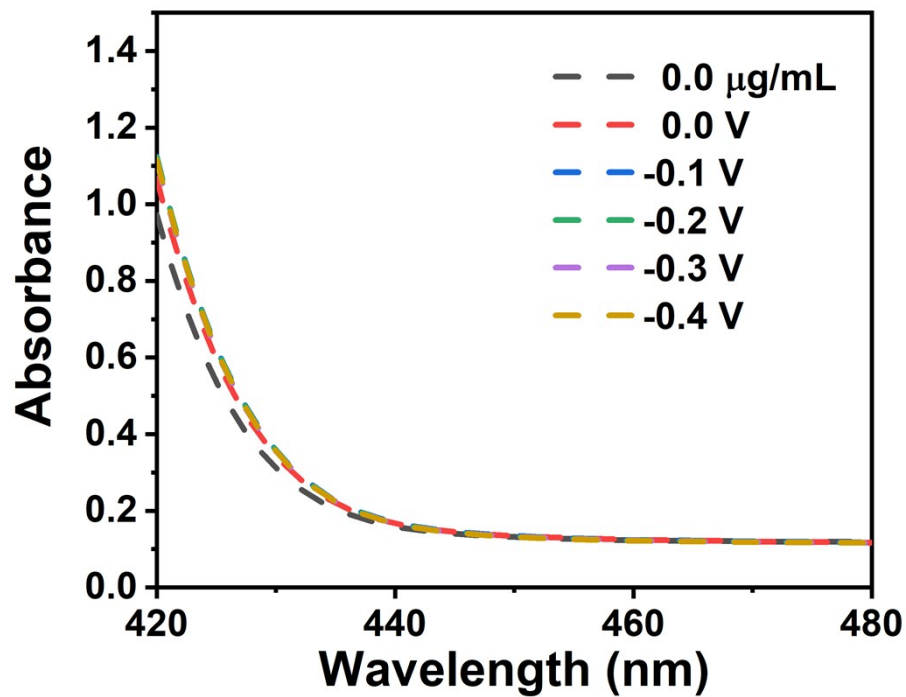


Fig. S6. UV-Vis absorption spectra of the electrolytes after NRR electrolysis at a series of potentials after incubated for 10 min at room temperature.

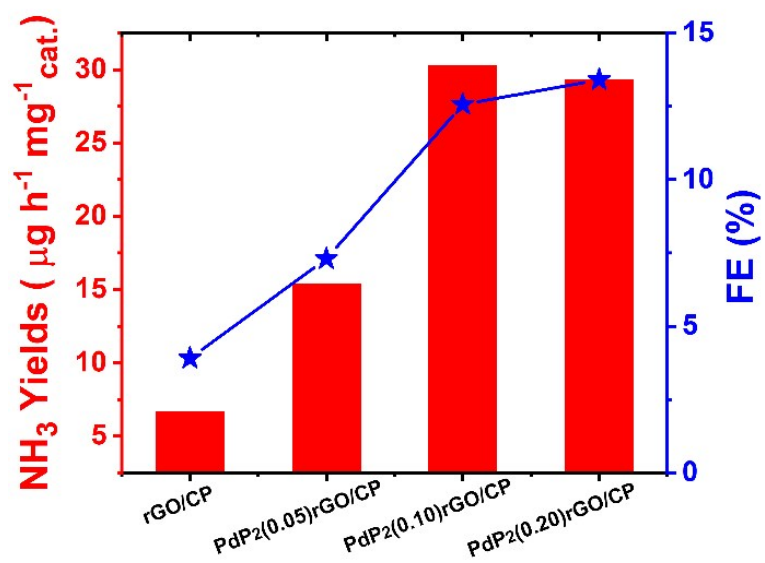


Fig. S7. NH₃ yields and FEs of PdP₂(x)-rGO at -0.10 V vs. RHE.

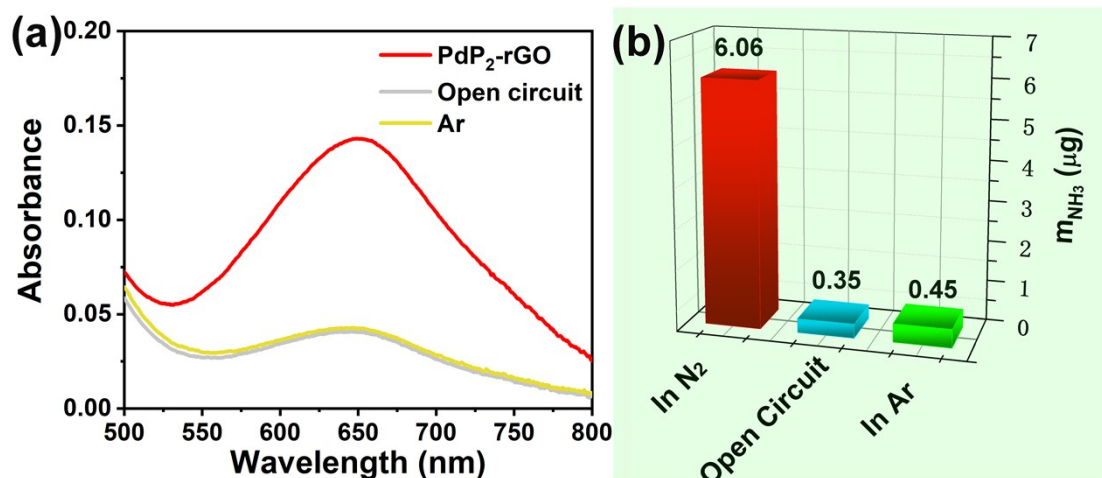


Fig. S8. (a) UV-Vis absorption spectra of the electrolytes stained with an NH₃ color agent under different conductions at -0.1 V. vs. RHE. (b) Amount of NH₃ generated of PdP₂-rGO/CP under different conductions at -0.1 V. vs. RHE.

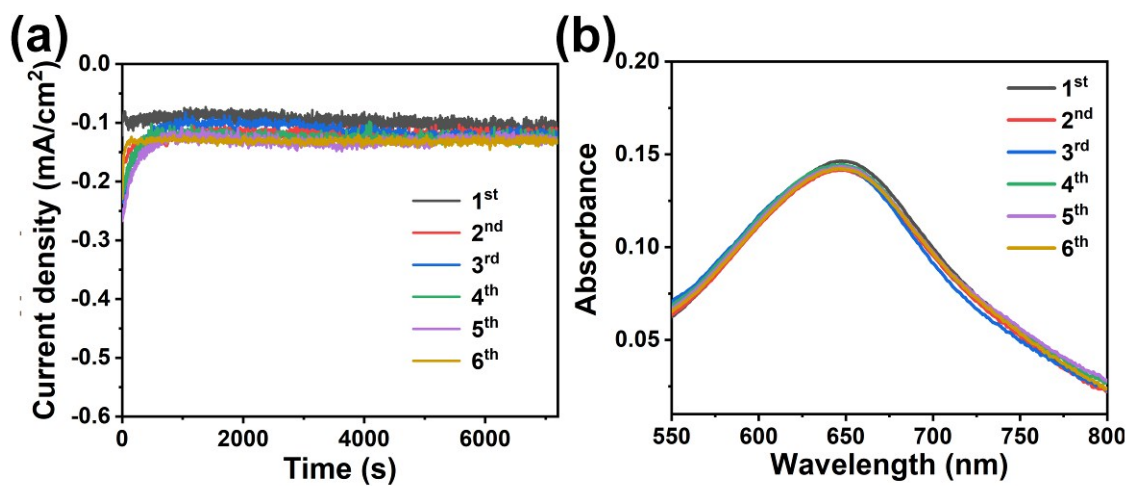


Fig. S9. (a) Time-dependent current density curves of PdP₂-rGO/CP at -0.1 V vs. RHE for continuous cycles. (b) UV-Vis absorption spectra of the electrolytes stained with an NH₃ color agent for continuous cycles.

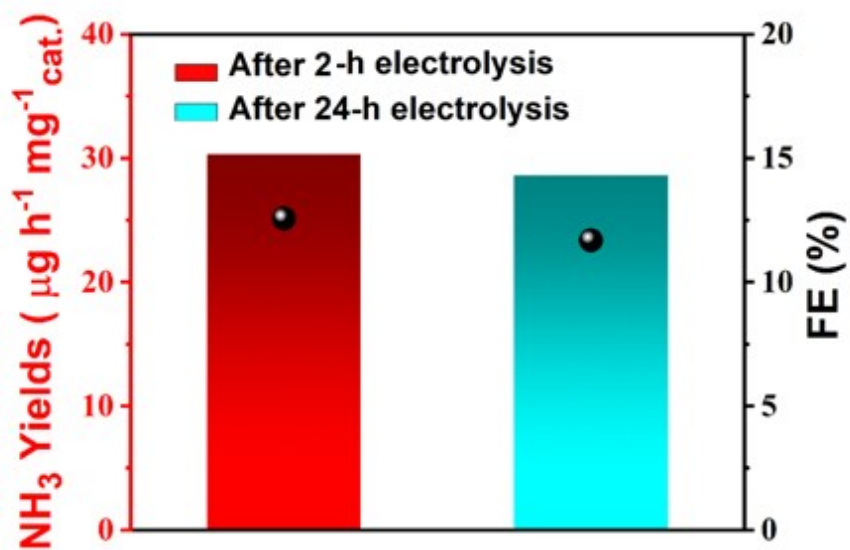


Fig. S10. NH₃ yields and FEs after charging at -0.10 V vs. RHE for 2 and 24 h.

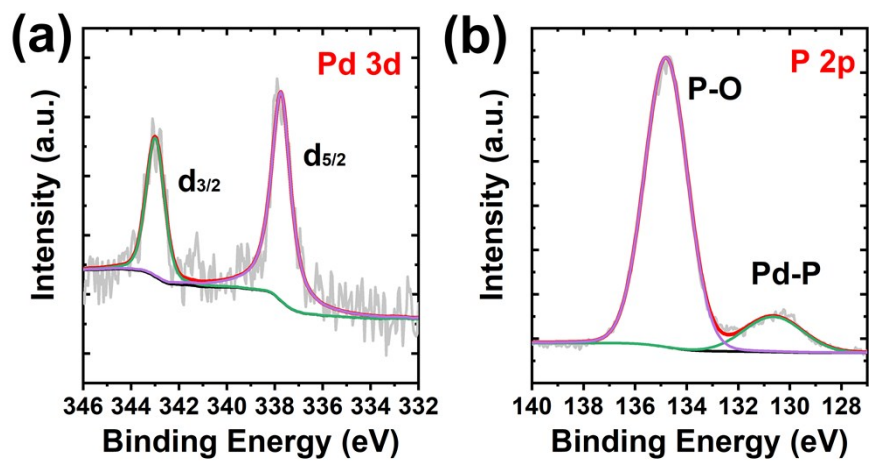


Fig. S11. XPS spectra of PdP₂-rGO after NRR test

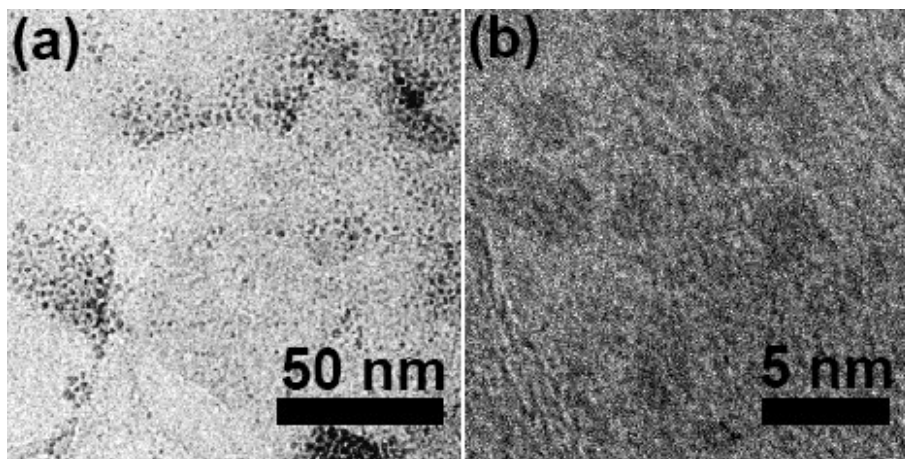


Fig. S12. TEM images of PdP₂-rGO after NRR test.

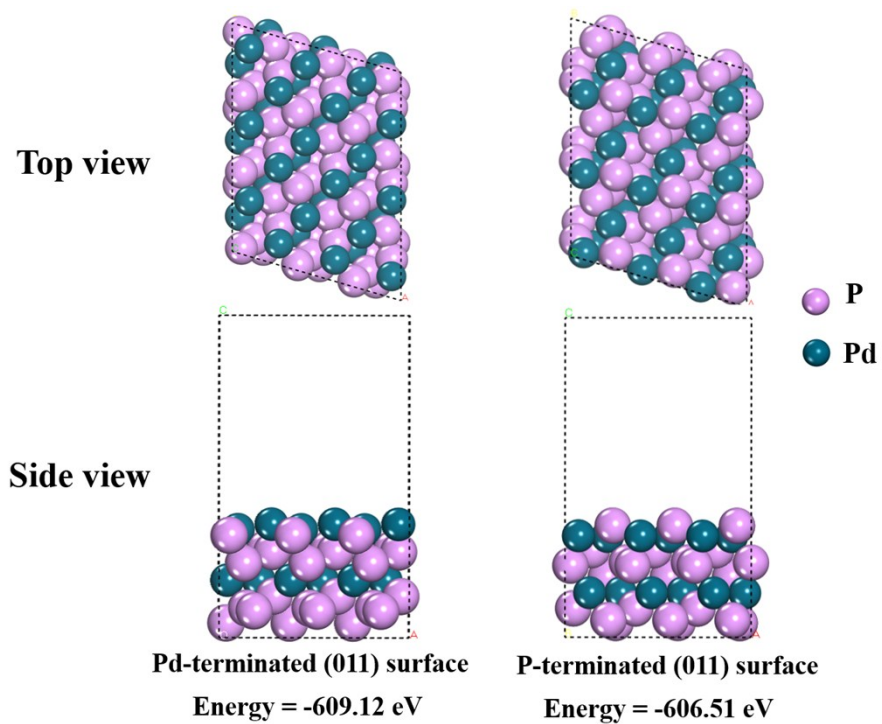


Fig. S13. Side and top views of the two optimized surface and its corresponding energy.

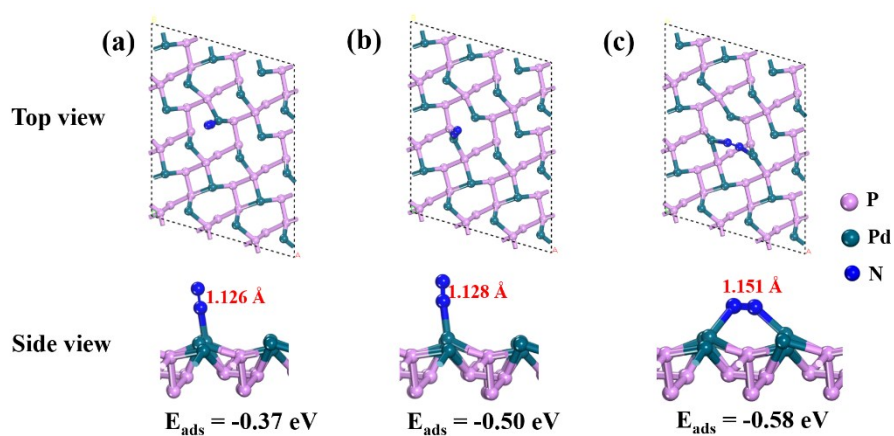


Fig. S14. Investigated N_2 adsorption geometries and its corresponding adsorption energy on the Pd-terminated PdP_2 (011) surface, (a) top site 1, (b) top site 2 and (c) bridge site, in which the value in red is the N–N bond length.

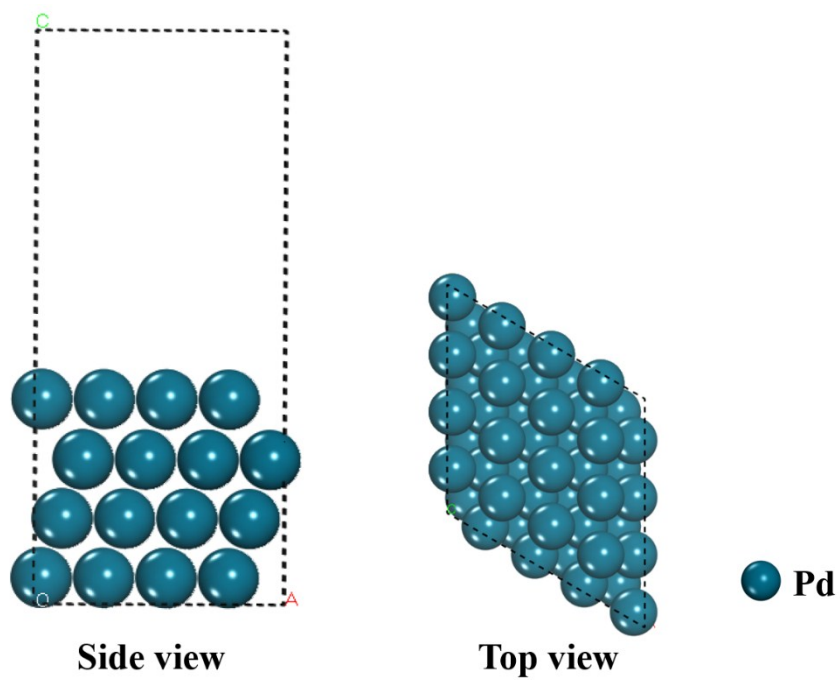


Fig. S15. Side and top views of the theoretical models of Pd (111) used in DFT calculations.

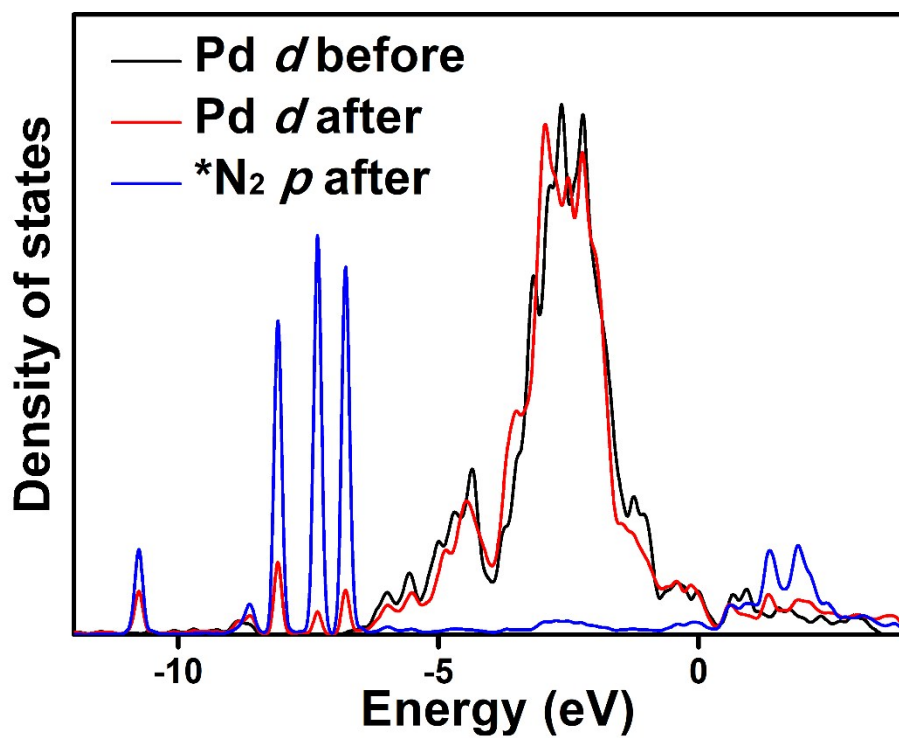


Fig. S16. Calculated partial density of state (PDOS) of the Pd (*d*) of PdP₂ before and after N₂ adsorption and N₂ (*p*) after adsorbed on PdP₂ surface. These PDOS are projected onto the Pd and N atoms which participate in the reaction.

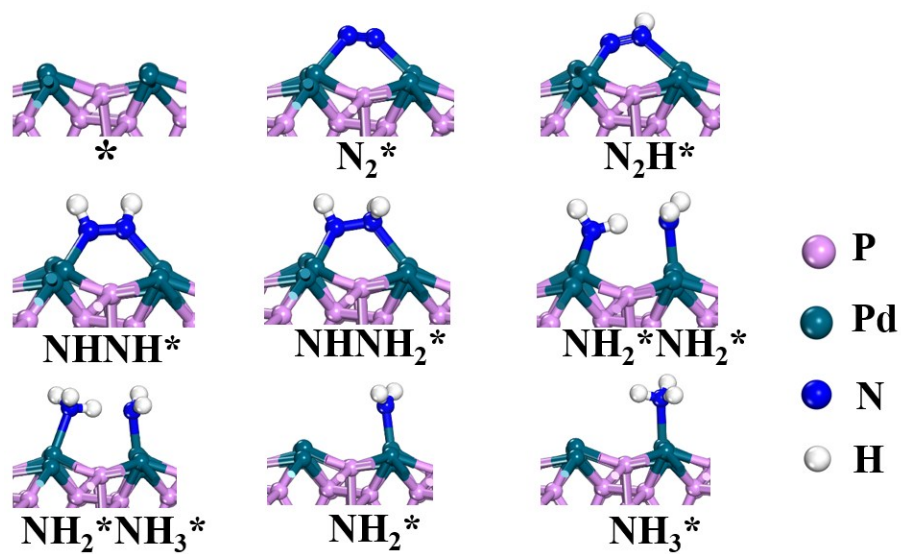


Fig. S17. Side view of optimized geometric structures of various intermediates along the reaction path of NRR proceeded on PdP₂ (011) surface through enzymatic mechanism.

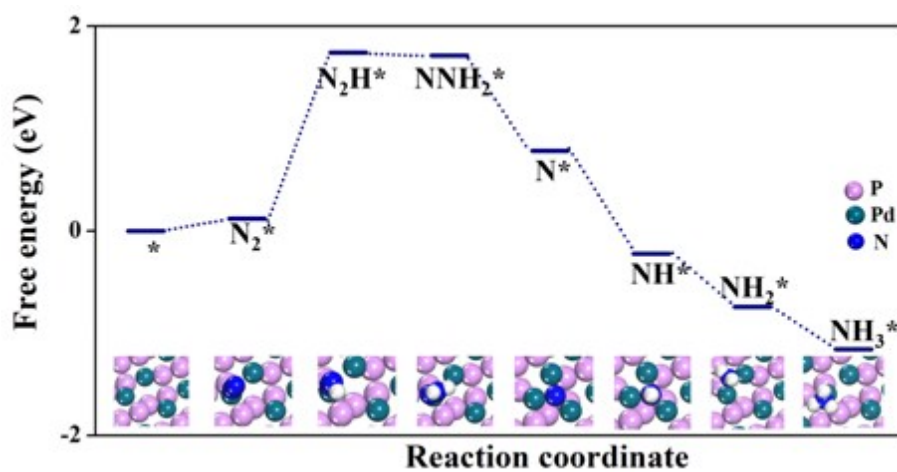


Fig. S18. Free energy diagrams for N₂ reduction through distal mechanism on PdP₂(011) surface at zero potential, together with optimized geometric structures of various intermediates.

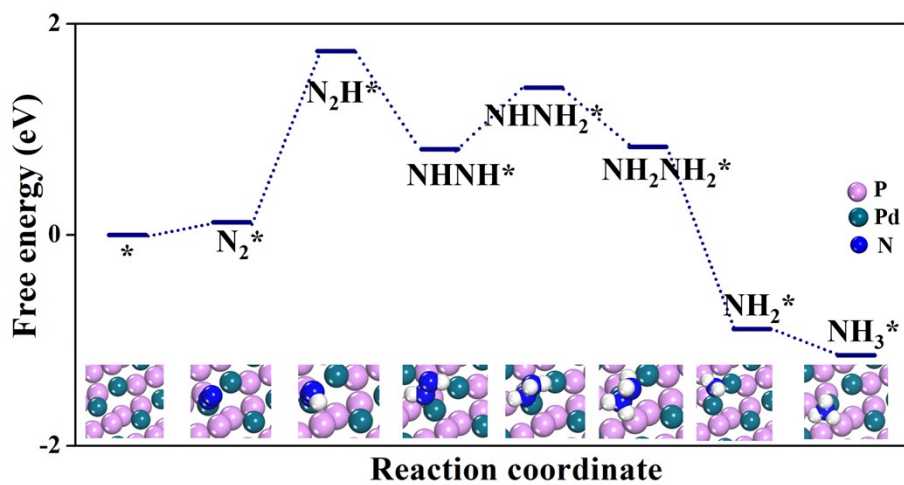


Fig. S19. Free energy diagrams for N₂ reduction through alternating mechanism on PdP₂ (011) surface at zero potential, together with optimized geometric structures of various intermediates.

Table S1. Comparison of the electrocatalytic NRR performance of PdP₂-rGO with other noble metal aqueous-based NRR electrocatalysts at room temperature.

Catalyst	Electrolyte	Potential	NH ₃ yield	FE	Ref.
PdP₂-rGO	0.5 M LiClO₄	-0.1 V	30.3 μg h⁻¹ mg⁻¹_{cat.}	12.56%	This work
Pd/C	0.1 M PBS	0.1 V	4.5 μg h ⁻¹ mg ⁻¹ _{cat.}	8.2%	9
PdCu-rGO	0.1 M KOH	-0.2 V	2.8 μg h ⁻¹ mg ⁻¹ _{cat.}	0.6%	10
PdRu tripods	0.1 M KOH	-0.2 V	37.23 μg h ⁻¹ mg ⁻¹ _{cat.}	1.85%	11
Pd-Co-CuO	0.1 M KOH	-0.2 V	10.04 μg h ⁻¹ mg ⁻¹ _{cat.}	2.16%	12
Au ₁ on N-doped porous noble carbon	0.1 M HCl	-0.2 V	2.32 μg h ⁻¹ cm ⁻²	12.3%	13
Au flowers	0.1 M HCl	-0.2 V	25.57 μg h ⁻¹ mg ⁻¹ _{cat.}	6.05 %	14
Ag nanosheets	0.1 M HCl	-0.6 V	4.62 × 10 ⁻¹¹ mol s ⁻¹ cm ⁻²	4.8%	15
Au sub-nanoclusters on TiO ₂	0.1 M HCl	-0.2 V	21.4 μg h ⁻¹ mg ⁻¹ _{cat.}	8.11%	16
Au/CeO _x -RGO	0.1 M HCl	-0.2 V	8.3 μg h ⁻¹ mg ⁻¹ _{cat.}	10.1%	17
AuHNCs	0.5 M LiClO ₄	-0.5 V	3.98 μg h ⁻¹ cm ⁻²	14.8%	18
porous Au film on Ni foam	0.1 M Na ₂ SO ₄	-0.2 V	9.42 μg h ⁻¹ cm ⁻²	13.36 %	19
Ru NPs	0.01 M HCl	-0.1 V	0.55 μg h ⁻¹ cm ⁻²	5.4%	20
Pd ₃ Cu ₁ alloy	1 M KOH	-0.15 V	39.9 μg h ⁻¹ mg ⁻¹ _{cat.}	1.56%	21

Reference

- 1 D. Zhu, L. Zhang, R. E. Ruther and R. J. Hamers, *Nat. Mater.*, 2013, **12**, 836–841.
- 2 G. W. Watt and J. D. Chrisp, *Anal. Chem.*, 1952, **24**, 2006–2008.
- 3 G. Kresse, J. Furthmüller, *Phys. Rev. B* 1996, **54**, 11169.
- 4 G. Kresse, D. Joubert, *Phys. Rev. B* 1999, **59**, 1758.
- 5 P. E. Blöchl, *Phys. Rev. B* 1994, **50**, 17953.
- 6 J. P. Perdew, J. Chevary, S. Vosko, K. A. Jackson, M. R. Pederson and D. Singh, C. Fiolhais, *Phys. Rev. B* 1992, **46**, 6671.
- 7 J. P. Perdew and Y. Wang, *Phys. Rev. B* 1992, **45**, 13244.
- 8 A. A. Peterson, F. Abild-Pedersen, F. Studt, J. Rossmeisl, and J. K. Nørskov, *Energy Environ. Sci.* 2010, **3**, 1311.
- 9 J. Wang, L. Yu, L. Hu, G. Chen, H. Xin and X. Feng, *Nat. Comm.*, 2018, **9**, 1795.
- 10 M. Shi, D. Bao, S. Li, B. Wulan, J.-M. Yan and Q. Jiang, *Adv. Energy Mater.*, 2018, **8**, 1800124.
- 11 H. Wang, Y. Li, C. Li, K. Deng, Z. Wang, Y. Xu, X. Li, H. Xue and L. Wang, *J. Mater. Chem. A*, 2019, **7**, 801–805.
- 12 W. Fu, Y. Cao, Q. Feng, W. R. Smith, P. Dong, M. Ye and J. Shen, *Nanoscale*, 2019, **11**, 1379-1385.
- 13 Q. Qin, T. Heil, M. Antonietti and M. Oschatz, *Small Methods*, 2018, **2**, 1800202.
- 14 Z. Wang, Y. Li, H. Yu, Y. Yu, H. Xue, X. Li, H. Wang and L. Wang, *ChemSusChem*, 2018, **11**, 3480–3485.
- 15 H. Huang, L. Xia, X. Shi, A. M. Asiri and X. Sun, *Chem. Commun.*, 2018, **54**, 11427–11430.
- 16 M. Shi, D. Bao, B. R. Wulan, Y. Li, Y. Zhang, J. Yan and Q. Jiang, *Adv. Mater.*, 2017, **29**, 1606550.
- 17 S. Li, D. Bao, M. Shi, B. Wulan, J. Yan and Q. Jiang, *Adv. Mater.*, 2017, **29**, 1700001.
- 18 M. Nazemi, S. R. Panikkanvalappil and M. A. El-Sayed, *Nano Energy*, 2018, **49**,

316–323.

- 19 H. Wang, H. Yu, Z. Wang, Y. Li, Y. Xu, X. Li, H. Xue and L. Wang, *Small*, 2019, **15**, 1804769.
- 20 D. Wang, L. M. Azofra, M. Harb, L. Cavallo, X. Zhang, B. H. R. Suryanto, and D. R. MacFarlane, *ChemSusChem*, 2018, **11**, 3416–3422.
- 21 F. Panga, Z. Wanga, K. Zhang, J. He, W. Zhang, C. Guo and Y. Ding, *Nano Energy*, 2019, **58**, 834–841.